Power Electronics and Drives
Volume 8(43), 2023 DOI: 10.2478/pead-2023-0015

Power Electronics and Drives

Multi-Step FEA-Based Design and Performance Analysis for a Single-Phase PM Brushless DC Motor

Research paper

Lidija Petkovska*, Goga Cvetkovski

Ss. Cyril and Methodius University, Faculty of Electrical Engineering and Information Technologies, Skopje 1000, North Macedonia

Received: 30, April 2023; Accepted: 04, July 2023

Abstract: In the article, an approach to design a novel single-phase permanent magnet (PM) brushless DC (BLDC) motor, based on multi-step FEA numerical prototyping, is presented. The designing procedure is carried out by using a series of 2D finite element simulations, until the design for a best performing PM BLDC motor is obtained. The proposed novel motor topology is developed using a generic motor, and through several steps, asymmetrical stator poles are devised, where one pair is particularly shaped. Permanent magnets are also simultaneously shaped. The aim of this research study is to improve performance characteristics of the motor by more efficient utilisation of active materials during the manufacture of rotor poles and stator cores. The magnetic field distribution in the motor cross-section, along with several other relevant electromagnetic and electromechanical characteristics, are computed, presented in figures and charts and analysed. The cogging torque and static torque waveforms, as well as the distribution of flux density and the air-gap flux, flux linkage and the induced back-emf, are in the focus of the presented research study. The results show that the novel design topology reveals featured operating characteristics, providing a smooth overall performance of the PM BLDC motor.

Keywords: *permanent magnet brushless DC motor • FEA-based topology design • back-emf • cogging torque • performance characteristics*

1. Introduction

Electric motors play a pivotal role in modern industrial and domestic applications. With the trends of more and smarter electric drives, the requirements for electric motors have become higher and higher, as for high power density at good thermal dissipation, high reliability, higher efficiency and reduced size and weight for lower active material consumption. Due to these new challenges in the last few decades, there has been a continuous interest for applications of brushless permanent magnet motors. This class of electric motors represents a variety of electrical machinery topologies with the highest torque density, which is ensured by the use of high-energy permanent magnets, such as NdFeB and SmCo types (El-Refaie, 2013). Their development and manufacturing have attracted a significant attention for extended applications, not only in electric drives but also in various industrial fields, including EVs/HEVs, renewable energy generation and aerospace, and various home appliances. Many efforts have been made to develop high-performance electric motors, such as with the application of novel electromagnetic materials (Guo et al., 2023b), modern control algorithms, advanced mathematical modelling (Königs et al., 2023; Ramakrishnan et al., 2017), numerical computations (Quintal-Palomo et al., 2016) and present-day optimisation design techniques (Guo et al., 2023a).

The electric motor optimisation is an evergreen topic. Its importance is increasing each year. Thus, the state of the art in electrical machine design is underlining the problems and challenges to be solved by researchers and engineers, even if the electric motor design is often considered a mature issue from the technical and technological point of view (Boglietti *et al*., 2014). In that sense, permanent magnet brushless DC (BLDC) motors is a recently

* *Email: lidijap@feit.ukim.edu.mk*

introduced research area for electrical machines because of their superior efficiency, relatively high torque density and high performance characteristics.

The class of single-phase permanent magnet (PM) brushless DC (BLDC) motors has been widely used in low-starting torque and low-power applications such as small pumps and cooling fans. These motors have a simple design and a lower manufacturing cost. Furthermore, single-phase permanent magnet BLDC motors offer possibility for compact and practical small-sized solutions with integrated drive electronics, which is a significant advantage when compared with their three-phase counterparts. However, these motors are perceived to have inferior self-starting ability, substantial cogging torque level and reduced starting torque at considerable torque ripples. The torque ripple is mostly subject to the motor drive design and is out of the scope of this study. The cogging torque is caused by the motor topology, which is due to the variation in the reluctance of the magnetic circuit during rotation. In particular, the alignment of the edges of the rotor and stator poles significantly contributes to this problem and is difficult to be avoided in a single-phase motor design. Indeed, without paying careful attention to the magnetic design, there will be starting and cogging torque issues with such motors. Therefore, recently, the topology of permanent magnet motors is under reconsideration, and new attractive designs for high-performance motors (Ferraris et al., 2015) with reduced cogging torque (Simón-Sempere et al., 2021) are being developed. Thus, the modularity of the design is introduced (Zhu and Li, 2018), while the asymmetric stator topology (Rezal and Ishak, 2019) enhances the performance of the PM motor. A specific class of PM BLDC machines are fractional-slot motors, which are characterised by a non-integer ratio of the number of stator slots to the number of rotor magnet poles (Wrobel and Mellor, 2008). Fractional-slot winding configurations in PM BLDC motors have attracted much attention because of the availability of more compact windings and low cogging torque (Yokoi et al., 2016).

The method that has been adopted for this research study involves an asymmetrical stator and a rotor magnet pole topology (Petkovska et al., 2022). The best ratio of stator asymmetry, determined by large pole arc vs. small pole arc, is chosen, while the rotor pole arc is taken the same as the smaller stator pole arc. With this arrangement, there is a compromise of achieving an acceptably low cogging torque, keeping the shape of the back EMF close to trapezoidal. The design and analysis tool used is the widely accepted finite element analysis (FEA) (Rupam et al., 2022). Thus, a thorough research, based on FEA, is accomplished and the novel PM BLDC motor design is proposed. The most relevant performance characteristics are calculated and presented in figures and charts, followed by comprehensive analyses. In this article, the results of this research are presented.

The article is organised as follows: a typical four-pole topology, followed by the brief step-by-step description of the prototype development of a single-phase PM BLDC motor is first presented. The analysis of the most important performance characteristics, that is, the magnetic field distribution and the cogging torque waveform follows. The next sections are dedicated to extended design considerations of this basic motor topology, until an original stator design of motor topology is contrived and the *novel PM BLDC motor* is proposed—the object of further comprehensive study. By exploiting FEM software, an accurate numerical approach to computation of the operating characteristics, an extensive performance analysis of the motor is carried out. The research results, presented in figures and charts, are discussed. Finally, conclusions are drawn.

2. Development of a Novel PM BLDC Motor

2.1. PM BLDC prototype motor

The research starts with investigating a typical four-pole topology of a single-phase permanent (PM) brushless DC (BLDC) motor, as presented in Figure 1, which is adopted as a *generic motor*. It is evident from the figure that inside the motor volume, a large amount of material is used for permanent magnets, as well as iron for the stator core lamination. This way, the utilisation of active materials is inefficient and costly. In addition, the large mass of permanent magnets will increase the rotor mass inertia and thus will worsen the dynamic behaviour of the motor, as well as will significantly increase the motor production cost.

Our aim is to redesign this generic motor topology and to transform it into a more practical model with more efficient material utilisation for permanent magnets and for stator cores, without deteriorating the waveform of the cogging torque characteristic, with as low as possible peak value, while also keeping the good motor performance features. To accomplish this objective, we propose a multi-step approach to solve the issues.

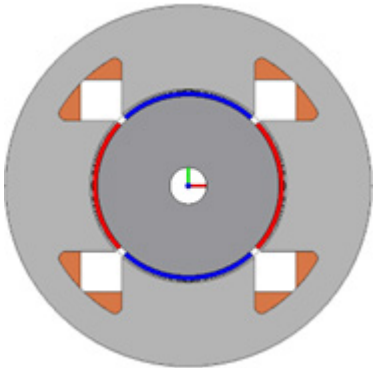

Fig. 1. Generic PM BLDC motor.

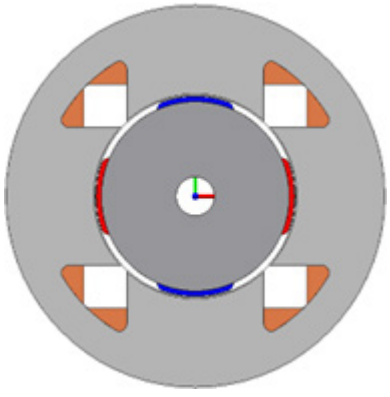

Fig. 2. Prototype PM BLDC motor.

Description	Value
Power supply	300 V @ 50 Hz
Rated phase current	3.3 A
Rated speed	1500 rpm
Input power	750 W
Shaft torque	2 Nm
Total number of turns of stator windings	648 turns
Phase resistance	6.987 Ω

Table 1. Rated Data of PM BLDC Motor.

Considering that the material for rotor magnets is the most expensive, first the permanent magnets are redesigned and decreased in size (Ling et al., 2016), while stator poles are taken the same as in the generic motor model; the preliminary test value of permanent magnet arcs is arbitrary selected 40°. This new modified motor topology of the generic motor, as shown in Figure 2, is adopted as a *prototype motor* and is a subject of the subsequent extensive research study. The PM BLDC prototype motor is manufactured and thoroughly examined at a laboratory test bench. The rated data of the motor and the main dimension, including used materials, are presented in Tables 1 and 2, respectively. The demagnetising characteristics B_r–H_c for the permanent magnet material and the magnetising characteristics B–H of electrical steel used for the stator and rotor core are presented in Figures 3–5, respectively.

At the beginning, the research interest of the authors is focussed on the shape of the cogging torque characteristic and its peak value (Petkovska and Cvetkovski, 2022). Cogging torque is a parasitic motor output and is certainly the most undesired occurrence in any PM motor performance. Cogging torque in permanent magnet motors is a predominant factor that influences the torque ripple level and the control precision (Hwang et al., 2018). It is

Description	Material/value
Stator core material	M350-50A
Rotor material	Cold rolled 1010 steel
Permanent magnets	BREMAG 10N (NdFeB)
Stator outside radius	76.6 mm
Stator inside radius	41 mm
Rotor outside radius	38 mm
Shaft radius	7.75 mm
Permanent magnet height	2 mm
Core length	54 mm
Stator pole body width	54.4 mm
Stator back iron thickness	14 mm

Table 2. Dimensions and Materials of PM BLDC Motor.

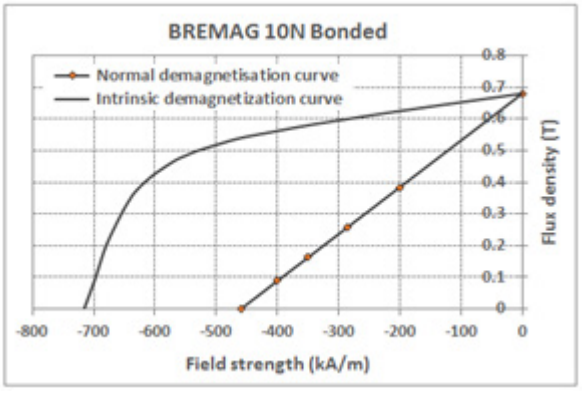

Fig. 3. Demagnetisation B_r–H_c curves for permanent magnets.

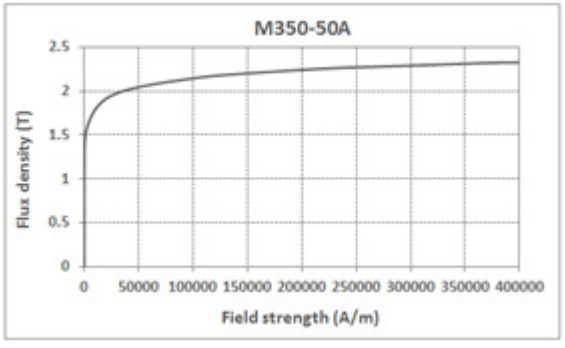

Fig. 4. Magnetising *B*–*H* curve for stator core.

produced due to the stator saliency, that is, due to the interaction between the rotor magnets and the stator slots/poles. As a computational tool, FEA-based numerical simulations are utilised. The results presented in the article are computed using 2D FEM code (Simcenter: MagNet Suite, 2019). To perform accurate FEM calculations, the detailed geometry dimensions of the motor design topology and properties of the used materials is a prerequisite. For consistency, the basic geometric dimensions and applied materials of the prototype PM BLDC motor (Figure 2), as presented in Table 2, are kept the same for all the subsequent design models.

To determine the cogging torque characteristics for the initial models—the generic PM BLDC motor and the prototype motor—separate FEM runs are carried out. Without current in stator windings, the rotor is displaced in

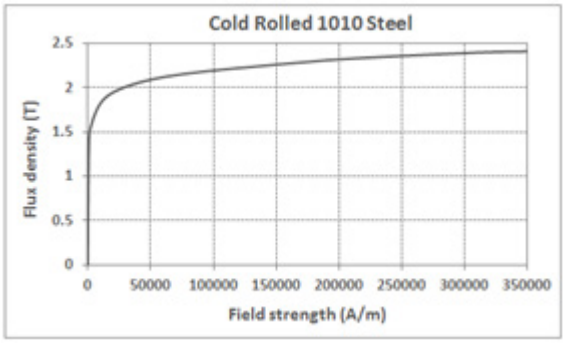

Fig. 5. Magnetising *B–H* curve for rotor core.

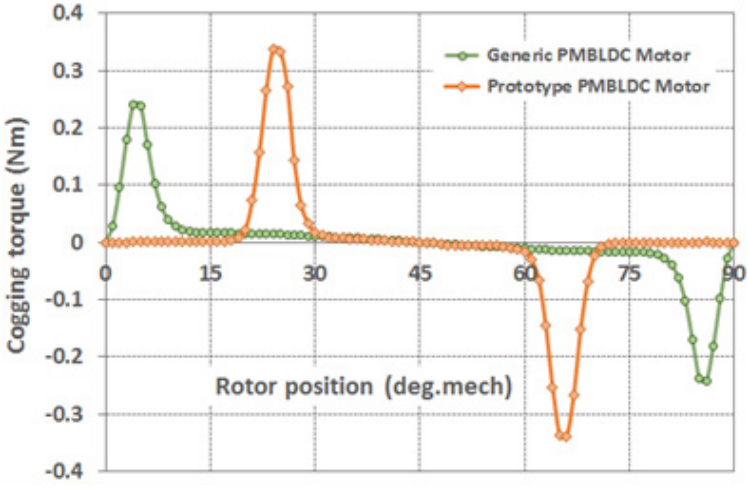

Fig. 6. Cogging torque profile for the generic and prototype PM BLDC motor.

steps, for an angle $\theta = 1°$ in the clockwise direction, and the cogging torque characteristic $T_{cog} = f(\theta)$ is numerically calculated. The characteristics, along one period of change 90° mech., are displayed in Figure 6, where the initial position of 0° is determined when the geometrical axes of permanent magnets and of stator poles are aligned.

Figure 6 shows that both motor models have a similar shape; however, the generic PM BLDC motor exhibits better features of its profile and is with lower peak value of 0.241 Nm. From the analysis of the figure, the following outcomes are seen: • reducing the PM size in the prototype motor, moves the position of peak cogging torque for 20° mech. in clockwise direction, same as the rotor rotation; • although the peak value of cogging torque is still relatively low 0.338 Nm, due to reduced permanent magnets size (decreased arcs) a considerable topology saliency is introduced, and consequently it is increased by 40.2%, compared to 0.241 Nm of the generic motor; this fact is certainly an undesirable occurrence.

The next objective of analyses are the flux linkage characteristics $\lambda = f(\theta)$ for the generic and for the prototype PM BLDC motor, along one pole pair pitch of 180° mechanical, as presented in Figure 7. The reduced PM arcs in the motor prototype lead to the flattening of the curve around the centre line of the stator poles.

To complete the assessment of those two PM BLDC motor designs, the characteristics of the back-emf *e* are calculated and graphed on a chart. According to Faraday's law, the back-emf produced in a winding or a coil is computed by numerically differentiating the flux linkage λ in a coil, or taking the derivative of the flux Φ and multiplying with the number of turns connected in series. Hence, the induced electromotive force in the stator coils, which are actually concentrated phase windings, is determined using the following equation:

$$e(t) = -\frac{d\lambda}{dt} = -W_c \frac{d\phi}{dt} \quad \text{(V)} \tag{1}$$

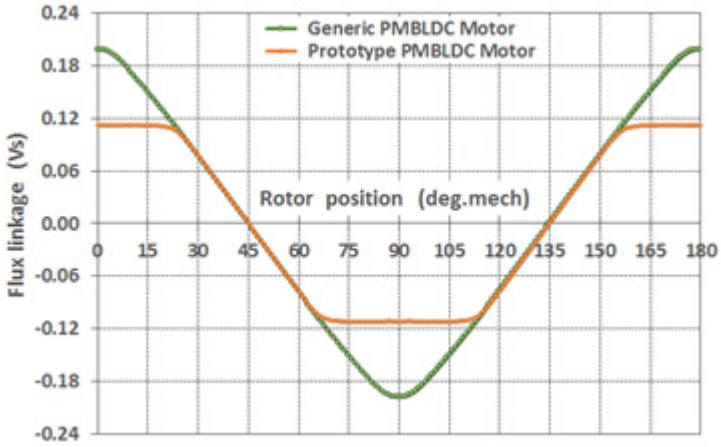

Fig. 7. Flux linkage characteristics for the generic and prototype PM BLDC motor.

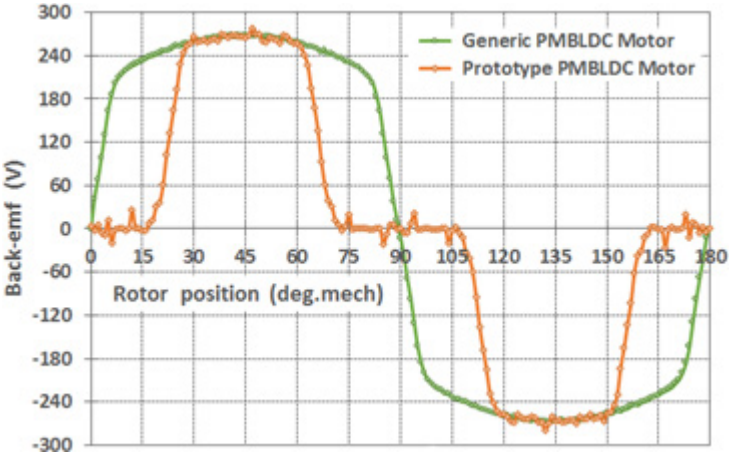

Fig. 8. Characteristics of the back-emf $e = f(\theta)$ for the generic and prototype PM BLDC motor.

Replacing the time variable t (s) with the angle of rotor displacement $\theta = f(t)$, for $n = n_n$, the following expression is derived:

$$e(\theta) = -W_c \frac{d\phi}{dt} = -W_c \cdot \frac{\Delta\phi}{\Delta\theta} \cdot \frac{\Delta\theta}{\Delta t} = -W_c \cdot \omega_n \cdot \frac{\Delta\phi}{\Delta\theta} \quad \text{(V)} \tag{2}$$

where W_c is the number of turns per pole coil, $\lambda = W_c \cdot \Phi$ (Vs) is the magnetic flux linked with the stator pole coil, θ (rad) is the angle of rotor displacement in the clockwise direction and $\omega_n = 2\pi n_n/60$ (rad/s) is the rated angular speed of the rotor, calculated for rated rotational speed n_n = 1500 rpm.

The characteristics $e = f(\theta)$, computed for the generic and for the prototype PM BLDC motor, are presented in Figure 8. The induced back-emf waveform for the prototype motor is affected by the reduction of the PM arc in a similar way as it was for the flux linkage characteristic. Namely, its flattened part, with almost no value change, results in almost zero value of the back-emf. The minor oscillations around the x-axis arise from the FEM-generated mesh size and respective sensitivity of the numerical derivatives for the flux on it.

2.2. Designing and shaping stator poles

Harnessing the authors' experience in the electric motors design, the further topology improvements for the studied motor are proposed and discussed. The original idea was to design a novel motor with an asymmetric stator, where the neighbouring pairs of stator poles would have different pole arc lengths. It is worth to point out that the built-in

PMs are all with the same arc length as the small stator poles. Consequently, in the *first designing step*, as shown Figure 2 of the prototype motor, one pair of stator poles will remain the same, while the other will be decreased in size and adjusted to have an arc corresponding with resized permanent magnets. The derived motor design at this stage is presented in Figure 9a.

The appearing gap between the two adjacent stator poles is significantly increased, the fact that will certainly worsen the cogging torque profile. To keep the same inter-pole gap of 6°, as in the generic and prototype motors, the arcs for the big stator pole pair should be increased for the same angle as the other (small) stator pole arcs are decreased. This modification of the prototype motor, entitled *A–B motor,* is displayed in Figure 9b. It consists of one pair big poles A with arc length α, and another pair small poles B with arc length β.

Figure 9b shows that the side-effect of this operation will be larger than the previous cross-section of the stator pole A, leading to even more inefficient utilisation of iron. On the other hand, due to this increased cross-section of the A stator pole body, it will certainly become unsaturated to a greater extent than was before. Thus, the issue with excessive iron usage for stator poles still exists, and hence, further investigations for enhanced designs of the PM BLDC motor are required.

To fully assess the features of the modified A–B prototype motor, its cogging torque characteristic is calculated under the same running condition as explained before. Figure 10 shows the cogging torque characteristics of the generic and prototype motors, as well as of the modified motor design, entitled A-B prototype motor. From the figure, it is evident that the A–B stator topology assures intended both the peak value and the profile for the cogging torque curve.

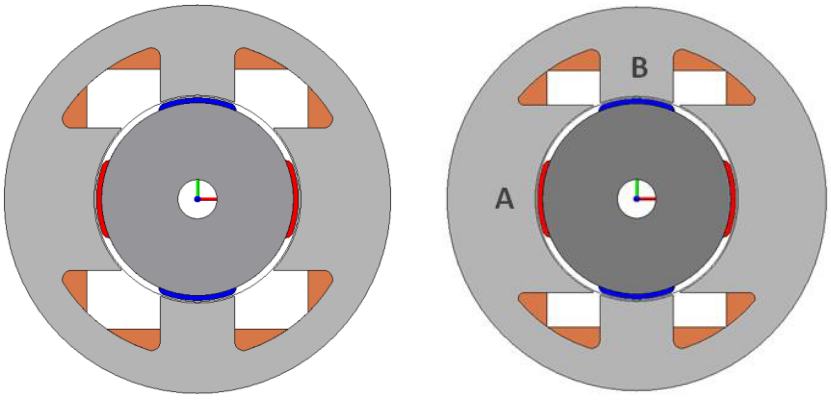

Fig. 9. Modifying the stator design of PM BLDC prototype motor. (a) first step of stator topology designing and (b) A–B prototype motor.

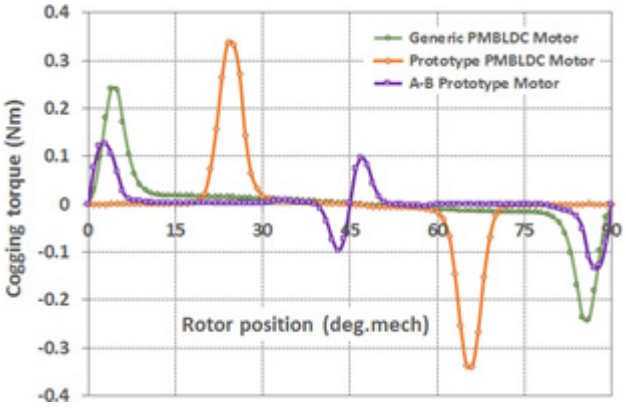

Fig. 10. Cogging torque profiles for the initial three models of PM BLDC motor.

The analysis of the characteristics in Figure 10 indicates the following: • the A–B prototype motor displays a shape closer to that of the generic motor; • the peak cogging torque is significantly reduced and is 0.126 Nm; • compared to the generic motor, the peak cogging torque of A–B prototype motor is 1.91 times lower, while compared to the prototype PM BLDC motor, the reduction is even more substantial, providing 2.68 times decrease; • the period of change is halved; • the motor A–B, designed according to the prototype modification procedure, showing smoother performance at the no-load operation, would be a solid basis for developing a *novel* single-phase PM brushless DC motor design.

To select the best arc ratio α/β of the large pole A and the small pole B, an investigative study on the modified A–B motor, based on extensive FEM calculations, is carried out. From the series of FE virtual prototyping, an arc $\beta = 42°$ for the small stator pole B and $\alpha/\beta = 3$ for the best value of the arc ratio are found. Consequently, the large stator pole arc is $\alpha = 126°$, while the gap between two adjacent stator poles remains to be 6°, as requested. The air-gap length along the stator bore is constant.

To accomplish one of the research objectives, that is, to achieve material saving for the stator core, in the next step, a part of the iron from the large stator poles is removed to design a classical *pole shoe* shape (Lefley et al., 2011), as denoted by a dotted line in Figure 11a. This intervention will also help create more winding space. To investigate and understand the effect of the proposed shape change, different pole shoe widths of the large stator pole A were implemented in the FE motor model. Using an unmodified stator pole (motor A–B) with an arc of 126° and uniform shape, denoted by full line in Figure 11a, a series of FEM simulations were performed by changing the radial pole shoe width from 6 mm to 12 mm. The magnetic field distribution and cogging torque profile are analysed. It is worth emphasising that the basic criterion is the saturation of the A pole neck and pole shoe, as well as of the stator yoke, to be avoided; the pole shoe width of 9 mm exhibited the best results. The geometrical cross-section of the novel stator design is shown in Figure 11b, where the parameters for FEM simulations are also indicated.

2.3. The novel PM BLDC motor

A generic motor comprises four concentrated windings around each pole, with a total of 648 turns, achieved by 162 turns/pole; hence, it is accepted to keep the same number of turns in the novel motor design. However, coil turns should be adjusted according to the different cross-sections of stator poles A and B. To obtain the smooth magnetic field distribution in the new motor topology, with similar flux density values in both poles A and B, coils with different numbers of turns for poles A and B are proposed. For this reason, the best fitted number of turns W_A and W_B need to be investigated. To properly define the respective values, an extensive work is required. In FEM-based numerical experiments, coil A is determined to have $W_A = 190$ turns/pole, while coil B is found to have $W_B = 134$ turns/pole. The final result of this complex multi-stage research is a contrivance of the *novel PM BLDC motor topology*. The 3D view of the *novel motor*, where the determined design parameters are indicated, is presented in Figure 12.

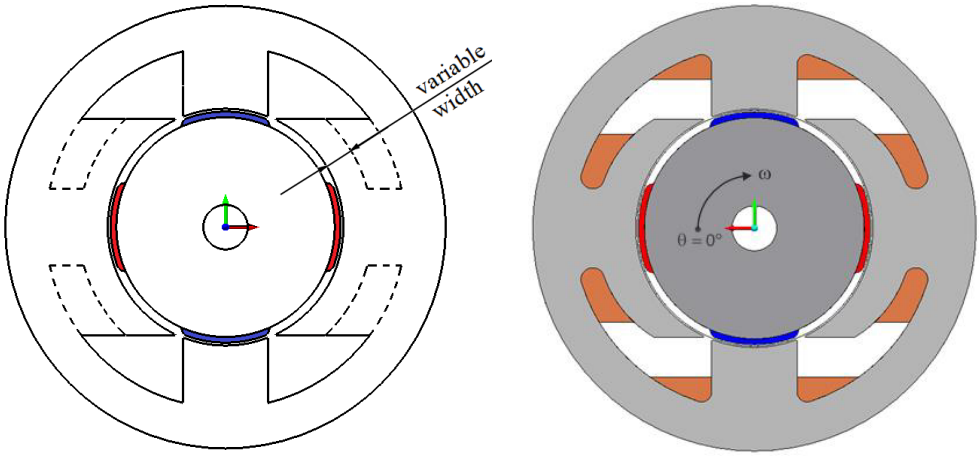

Fig. 11. Designing and shaping the stator of PM BLDC motor. (a) shaping the big stator poles and (b) the novel motor topology.

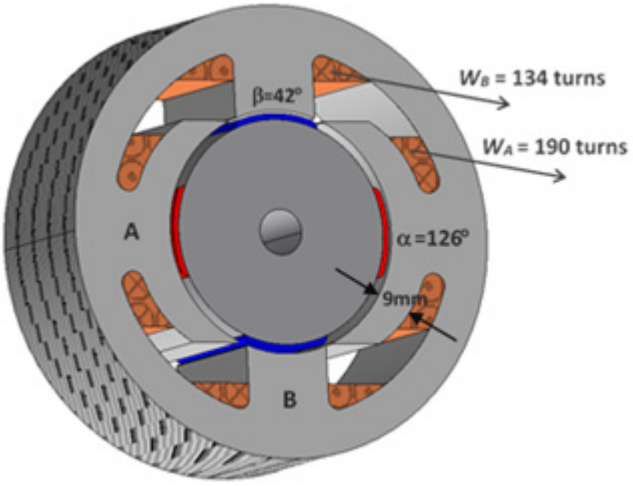

Fig. 12. 3D view of the novel PM BLDC motor design.

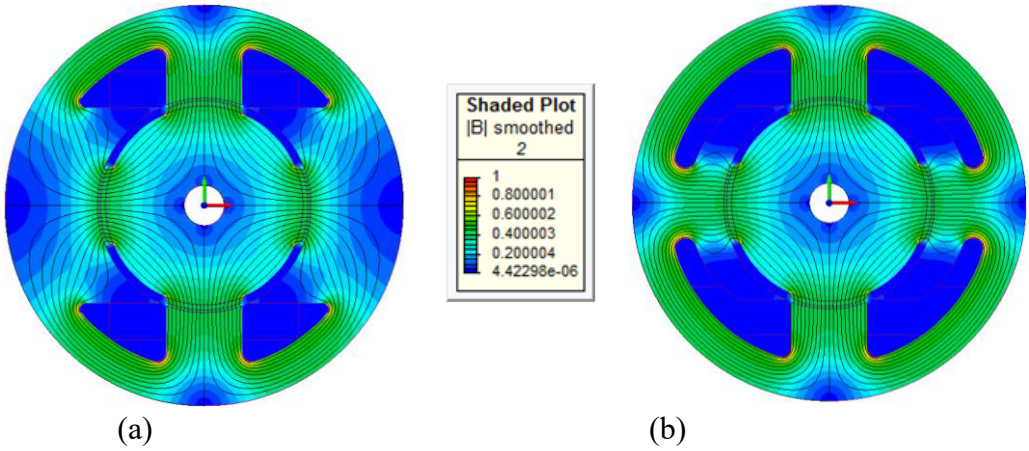

Fig. 13. Magnetic flux distribution at no-load. (a) A–B prototype motor and (b) Novel motor.

3. Evaluation of the Novel PM BLDC Motor

The proposed *novel PM BLDC motor*, being derived from *the generic motor* through the A–B *prototype motor*, by designing and shaping the large stator poles, will certainly have different operating characteristics. To evaluate the performance of the novel motor design, the aforementioned A–B motor and the novel motor are analysed in parallel. Using FEA as well established numerical tool (Ocak et al., 2017), the electromagnetic and electromechanical characteristics for the both novel PM BLDC motor and the A–B prototype motor are computed and studied. The initial rotor position, defined with the angle $\theta = 0°$, is selected when the stator pole axes are aligned with permanent magnet axes, as shown in Figure 11b, where the motor rotates in the clockwise direction. The no-load and rated load operating regimes are considered and investigated. Magnetic field distribution and the respective torque characteristics are computed and presented in figures and charts.

3.1. No-Load operation and cogging torque

Magnetic flux distribution at the no-load operation is obtained when the magnetic field of the motor is energised by the permanent magnets only. Flux lines at the selected initial position, for the A–B prototype motor and the novel motor, are presented in Figures 13a and b, respectively. It is evident that the stator pole saturation is of the same level, although a huge amount of iron mass of the large pole body in the novel motor is removed.

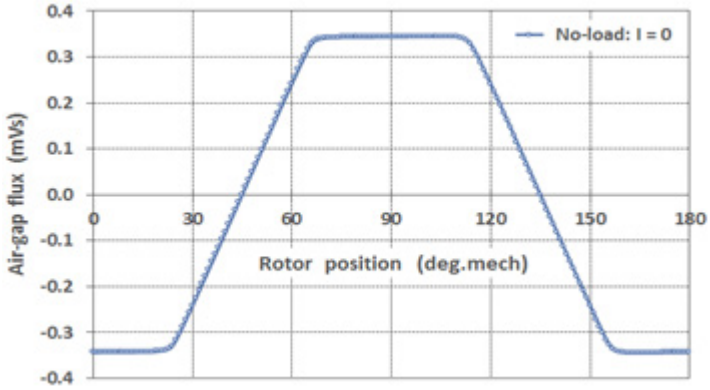

Fig. 14. Air-gap flux distribution along mid-gap line of the novel PM BLDC motor at no-load.

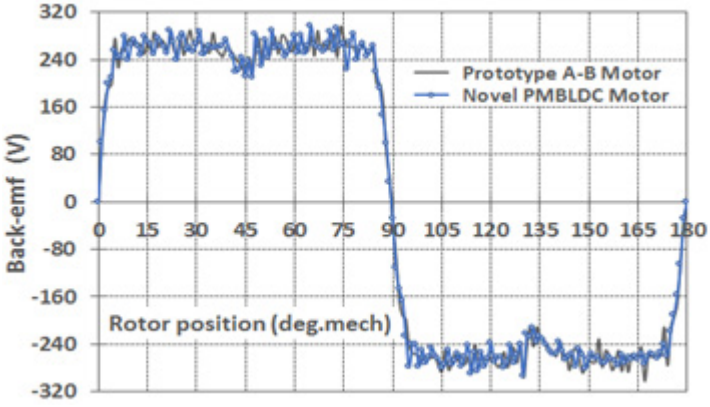

Fig. 15. Back-emf characteristics for A-B prototype motor and novel PM BLDC motor.

Using the FEM results at the no-load operation of the novel motor, the air-gap magnetic flux is determined, and the flux chart, in dependence of the rotor position along one pole pair, is presented in Figure 14. The shape of the characteristic is almost ideally trapezoidal, which is one of the most desired features of PM BLDC motors. Hence, it is worth emphasising that this is one of the objectives to be achieved in this research study. Following the same procedure demonstrated in Heading 2.1, the back-emf for the A-B prototype motor and novel PM BLDC motor is computed; their characteristics are presented comparatively in Figure 15.

The no-load operating regime, when the rotor is freely changing the position, enables the calculation of the cogging torque characteristic, spanned over one pole pitch of 90° mechanical. Comparative cogging torque characteristics for the two previously studied designs are presented in Figure 16. The improvements of the novel PM BLDC motor design are evident. Apart from the iron saving for stator construction, due to the shaping A poles, the cogging torque profile remains identical as before in the A-B prototype motor (Figure 10). Even more, in the sections where $\theta \in (30°, 40°)$ and $\theta \in (75°, 80°)$, the novel motor exhibits smoother change. Moreover, the peak torque of the novel motor is 0.124 Nm, which is less than of the A-B prototype, whose peak torque is 0.126 Nm, showing a decrease of 1.5%.

3.2. Rated load operation and static torque

To evaluate the full performance of the novel motor, a series of FEM computations have been performed at loading conditions. The mesh of the novel PM BLDC motor is depicted in Figure 17; the mesh consists of around 15000 nodes and is particularly dense in the air-gap where the magnetic field is changing at the highest rate. The first calculations are performed for rated current I_n = 3.3 A, at the initial rotor position 0° when the armature field and PM field are aligned; the magnetic field distribution is presented in Figure 18. One can notice a reasonable level of saturation, even in the pole body from which an important part of iron has been removed. To add, the maximum

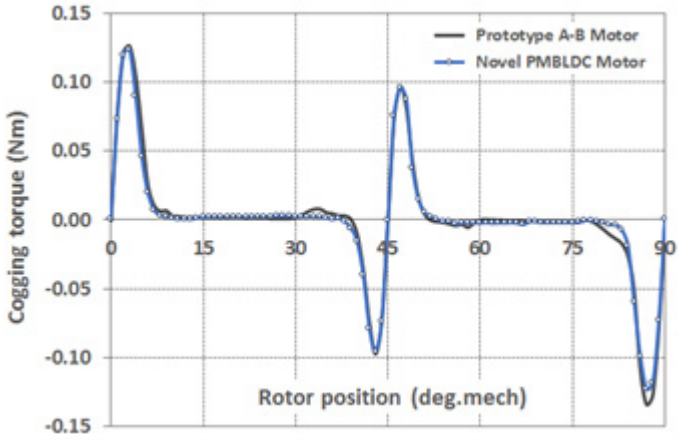

Fig. 16. Cogging torque comparative characteristics.

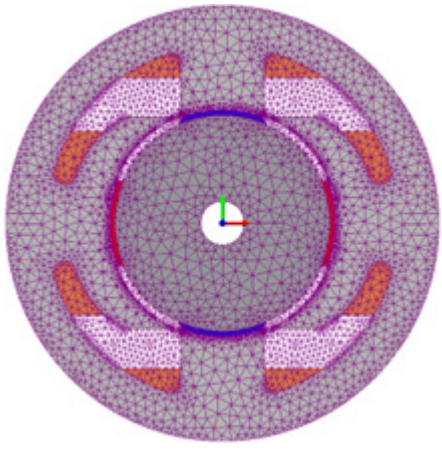

Fig. 17. Meshing PM BLDC motor.

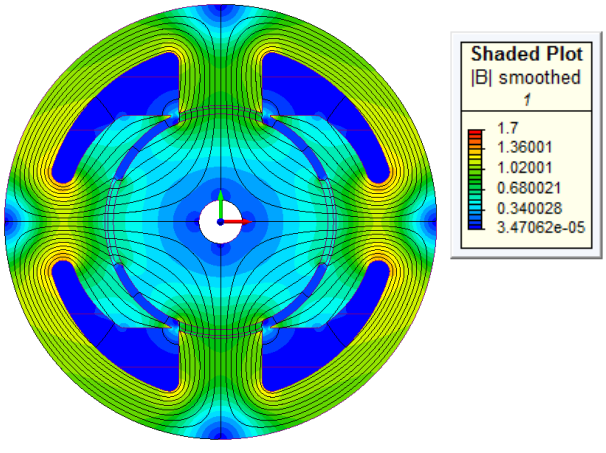

Fig. 18. Flux plot at initial position 0° and rated load I_n.

allowed flux density of 1.7 T in the stator yoke cross-section is not surpassed; hence, the utilisation of iron in the novel motor is more effective. This confirms that during the procedure for improving the A–B prototype motor and designing the novel PM BLDC motor, another research goal has been achieved.

Two typical rotor positions are also analysed. The first position is when the north rotor pole axes point in the middle of inter-pole gaps, equivalent to the displacement in the CW direction for 24° mech., and another is for rotor displacement of 45° mech., equivalent to 90° el. in the same direction. Owing to comparable magnetic field results, the same scale is used for the plots as before, where the maximum flux density is set at the value of 1.7 T. Magnetic field distributions at rated current I_n = 3.3 A in the armature windings and for those two rotor positions are presented in Figures 19a and b, respectively. The saturation level of the stator back-iron is quite low, while the most saturated parts of pole shoes are still at an acceptable high level.

The load operating regimes enable the calculation of the electromagnetic and electromechanical characteristics of the novel PM BLDC motor. The FEM computations are carried out for different armature currents and at different rotor positions, along the air-gap circumference. The armature current is changed from zero up to the rated value in several predefined steps, while the rotor position is changed quasi-statically for 1° along one period of 0–180° mech. A series of numerical calculations have been accomplished. The flux density distribution corresponding to the rotor position change along the middle air-gap line, at no-load and at rated load operations, is shown in Figure 20.

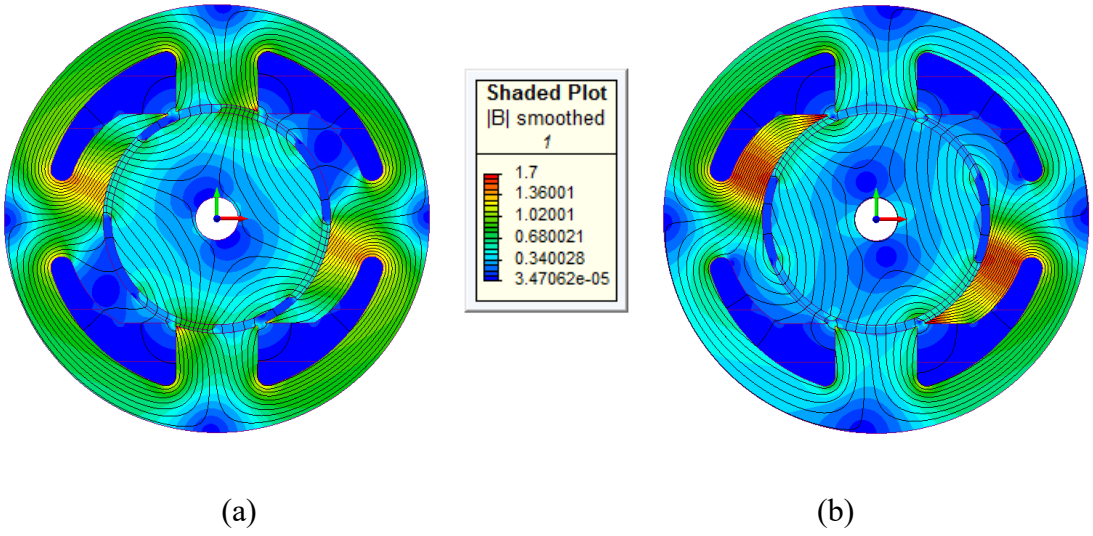

Fig. 19. Magnetic flux distribution of the novel motor at rated current I_n: (a) rotor position 24° in CW direction and (b) rotor position 45° in CW direction.

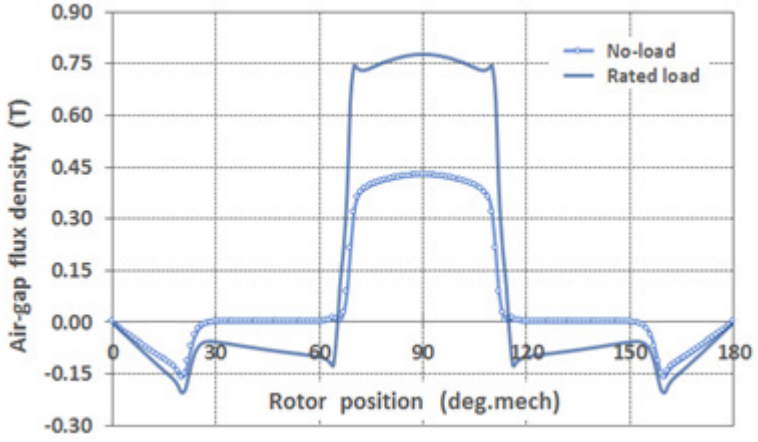

Fig. 20. Flux density distribution along the mid-gap line for $I = 0$ and $I = I_n$.

Figure 21 presents the characteristics of the instantaneous values for the first half-period, that is, 0° – 90° mechanical, which is used to examine the properties of the induced back-emf for the novel PM BLDC motor. The dotted line on the chart shows the averaged values and points out the quite desirable shape for the back-emf.

The static electromagnetic torque characteristics are computed for armature currents in a range of 0–3.3 A, varying the rotor position 0°–180° along one pole pair pitch. The characteristics T_{em} = f(θ) for rated current I_n and for current $I = I_n/2$ along one full period of change are shown in Figure 22. Figure 23 presents the static torque characteristics T_{em} = f(I) for two typical rotor positions (24° and 45°), corresponding to Figures 19a and b.

To encompass the research work presented here, the static torque characteristics of the novel motor PM BLDC motor in comparison with the A-B prototype motor are analysed; the characteristics for a half-period of change (90° mech.) are presented in Figure 24.

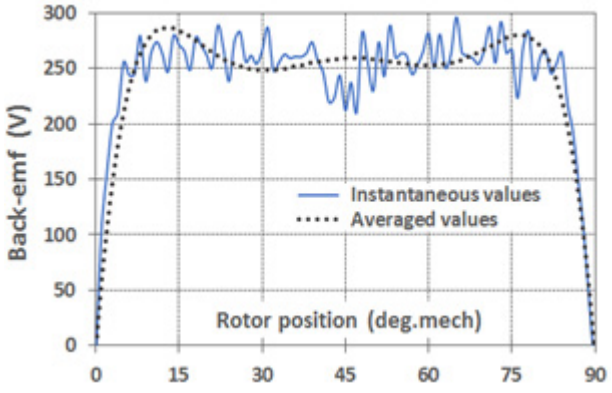

Fig. 21. Instantaneous and averaged back-emf characteristic of novel PM BLDC motor.

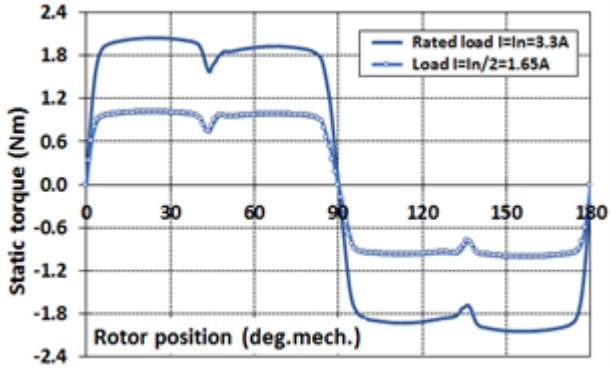

Fig. 22. Torque characteristics T_{em} = f(θ) of the novel PM BLDC motor.

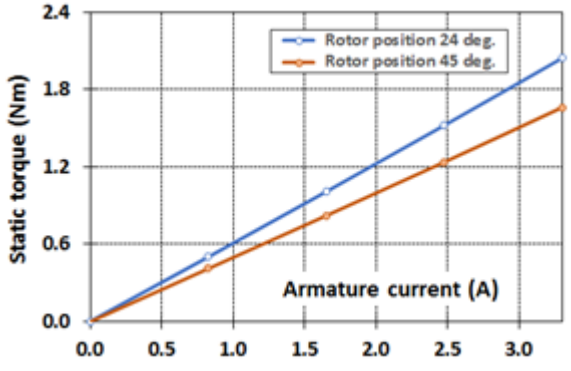

Fig. 23. Torque characteristics T_{em} = f(I) of the novel PM BLDC motor.

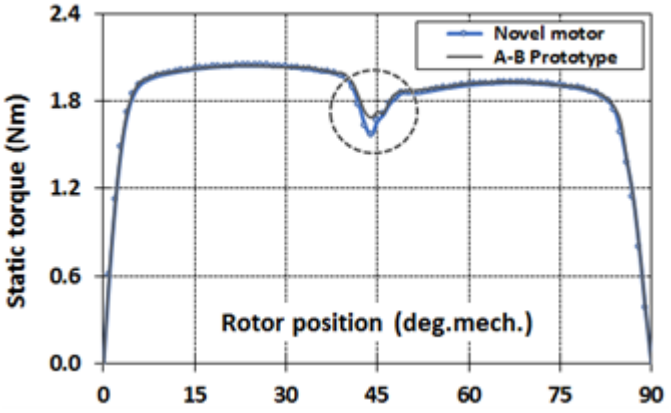

Fig. 24. Comparative static torque characteristics at rated current I_n.

The static electromagnetic torque of the novel motor, similar to the cogging torque, has an identical waveform as the A–B prototype. The only evident difference, which is not in favour of the novel motor design, is a slightly greater drop around the angle 45° mech. ≡ 90° el., as shown in Figure 24. However, it is worth emphasising that in general, PM BLDC motors are not allowed to ever reach this working point. To summarise, it is definitely proved that in whole, the novel motor performance is improved, and hence, the purpose of the presented research work and corresponding goals have been successfully accomplished.

3.3. Summary of the novel PM BLDC motor features

First, the attributes of the proposed novel PM BLDC motor topology design are briefly summarised as follows:

- the arc of 42° for the rotor magnets is determined, saving the material and cost for their production;
- the two stator pole pairs—large A and small B—are of different arc lengths, where the arc of B pole is equal to the PM arc of 42°;
- the large A pole arc is 3 times the length of the small B pole arc, that is, an angle of 126°;
- consequently, the inter-pole gap of 6° is kept the same as in the generic motor model and is sufficient for easy inserting the stator coils during motor manufacturing;
- the number of turns per pole, accordingly to their different sizes and shapes, is different; $W_A = 190$ turns per A poles and $W_B = 134$ turns per B poles are determined.
- the pole shoe of the large A pole is shaped with a thickness of 9 mm for creating more winding space and for saving iron utilisation, without exceeding the allowed level of saturation;
- thus, by increasing the magnitude of the flux in the A pole body and keeping the reasonable level of saturation, a notably better usage of active materials is achieved;
- all these unique features when combined together result in a *novel design of a PM BLDC motor*.

Extensive FEM-based numerical calculations for the proposed *novel motor* and for the A–B *prototype motor* are carried out, their operating characteristics are computed and presented comparatively, and a comprehensive FEA is accomplished. The overall performance of the novel PM BLDC motor and its operating characteristics are substantially improved, in such a way that:

- the trapezoidal characteristic of the air-gap flux is generated;
- the waveform of the induced back-emf is quite favourable;
- the peak value of the cogging torque 0.124 Nm is slightly decreased compared to A–B prototype, and is lower for 1.5%, while the profile is smoother;
- it is worth to point out that it decreased by 94.4% compared to the generic motor, while with reference to the prototype motor, it is lower by 2.73 times, which is the reduced peak value for 173%;
- the static torque characteristic is flat stable shape, providing self-starting of the motor and reliable steady operation at load;

– the only drawback that might be considered is the relatively low value of static electromagnetic torque, and the next foreseen research challenge will be to investigate the techniques for increasing the torque and improving the motor performance at load, keeping the advantages gained so far.

4. Conclusion

The contribution of this article is to demonstrate how the FEA-based numerical tool for virtual prototyping could be implemented in a motor designing procedure. This article presents a multi-step design for a single-phase permanent magnet (PM) brushless DC (BLDC) motor, starting from a generic motor topology. The objective of this research study was to improve the motor overall performance by more efficient utilisation of the active materials for manufacturing the rotor PM poles and the stator iron core. The novel motor topology is developed through several steps, where a specific A–B prototype motor with asymmetrical stator pole pairs—large A and small B—is first devised, and the permanent magnets are simultaneously resized and shaped. Afterwards, aiming to more effective usage of active materials, stator poles A are redesigned; an important part of the pole body is removed, in a way that they get particularly shaped pole shoe, without deteriorating the magnetic saturation. The flux plots in both motor models, A–B and novel, prove the accomplishment.

The most relevant operating characteristics for the A–B prototype motor and the designed novel PM BLDC motor are numerically computed, comparatively presented on charts and discussed. After a comprehensive analysis is accomplished, it can be noted that the overall performance of the novel PM BLDC motor is substantially improved.

In the future, the authors intend to investigate the possibilities offered by state-of-the-art production technologies for electric motors. The key idea will be to exploit the promising features of novel magnetic materials, such as soft magnetic composites (SMCs), and to design a PM BLDC motor with smooth waveforms of cogging and electromagnetic torque characteristics. The aim will be to increase the rated value of the static torque, while keeping the features of the cogging torque characteristic identified in this study. This will help implement the advantages of modern production technologies, which in turn will ultimately result with a design and production of an attractive single-phase permanent magnet brushless DC motor. This article will serve as a solid basis and a comprehensive guide to design a novel single-phase PM BLDC motor.

References

Boglietti, A., El-Refaie, A. M., Drubel, O., Omekanda, A. M. and Bianchi, N., Agamloh, E. B., Popescu, M., Di Gerlando, A. and Borg Bartolo, J. (2014). Electrical Machine Topologies: Hottest Topics in the Electrical Machine Research Community. *IEEE Industrial Electronics Magazine,* 8(2), pp. 18–30. doi: 10.1109/MIE.2013.2294077.

El-Refaie, A. (2013). Fractional-slot concentrated-windings: A paradigm shift in electrical machines. In: *2013 IEEE Workshop on Electrical Machines Design, Control and Diagnosis (WEMDCD)*, Paris, France, 11-12 March 2013, pp. 24–32. doi: 10.1109/WEMDCD.2013.6525162.

Ferraris, L., Franchini, F. and Poskovic, E. (2015). Design optimization of bonded PM BLDC motors with reference to the cogging torque amplitude. In: *Proceedings of the 41st Annual Conference of the IEEE Industrial Electronics Society*, Yokohama, Japan, 9–12 November 2015, pp. 001264–001269.

Guo, L., Wang, Y., Wang, H. and Zhang, Z. (2023a). Design of High Power Density Double-Stator Permanent Magnet Synchronous Motor. *IET Electric Power Applications*, 17(4), pp. 421–431. doi: 10.1049/elp2.12275.

Guo, Y., Ba, X., Liu, L., Lu, H., Lei, G., Yin, W. and Zhu, J. (2023b). A Review of Electric Motors with Soft Magnetic Composite Cores for Electric Drives. *Energies*, 16, p. 2053. doi: 10.3390/en16042053.

Hwang, M.-H., Lee, H.-S. and Cha, H.-R. (2018). Analysis of Torque Ripple and Cogging Torque Reduction in Electric Vehicle Traction Platform Applying Rotor Notched Design. *Energies*, 11(11), p. 3053.

Königs, M., Baccouche, H., Breser, S., Jöns, T. and Löhlein, B. (2023). Simulation Time Reduction with 2.5D FEM-Analysis for Axial Flux Machines. *Power Electronics and Drives*, 8(43), pp. 100–108.

Lefley, P., Petkovska, L. and Cvetkovski, G. (2011). Optimisation of the design parameters of an asymmetric brushless DC motor for cogging torque minimisation. In: *Proceedings of 14th International European Conference on Power Electronics and*

Applications (EPE), Birmingham, United Kingdom, 30 August – 1 September 2011, pp. 1–8 on CD.

Ling, P., Ishak, D. and Tiang, T. L. (2016). Influence of magnet pole arc variation on the performance of external rotor permanent magnet synchronous machine based on finite element analysis. In: *Proceedings of IEEE International Conference on Power and Energy (PECon)*, Melaka, Malaysia, 28-29 November 2016, pp. 552–557.

Ocak, C., Dalcalı, A., Celik, E. and Uygun, D. (2017). FEA-Based Design Improvement of Small Scale BLDCMs Considering Magnet Thickness and Pole Embrace. *International Journal of Computing, Communication and Instrumentation Engineering*, 4(2), pp. 31–35.

Petkovska, L. and Cvetkovski, G. (2022). Optimising stator design of a single phase PM BLDC motor for improved cogging torque profile. In: *Proceedings of 8th International Symposium on Applied Electromagnetics (SAEM)*, Struga, North Macedonia, 26–29 June 2022, pp. 59–65.

Petkovska, L., Lefley, P. and Cvetkovski, G. (2022). Shaping the Topology of a Single Phase BLDC Motor for Reduced Cogging Torque and Improved Performance. *The European Physical Journal, Applied Physics*, 97(id.36), 8p.

Quintal-Palomo, R. E., Gwoździewicz, M. and Dybkowski, M. (2016). Parametric Analysis for the Design of a 4 Pole Radial Permanent Magnet Generator for Small Wind Turbines. *Power Electronics and Drives*, 1(36)(2), pp. 175–186. doi: 10.5277/PED160211.

Ramakrishnan, K., Curti, M., Zarko, D., Mastinu, G., Paulides, J. J. H. and Lomonova, E. A. (2017). Comparative Analysis of Various Methods for Modelling Surface Permanent Magnet Machines. *IET Electric Power Applications*, 11(4), pp. 540–547. doi: 10.1049/iet-epa.2016.0720.

Rezal, M. and Ishak, D. (2019). Performance Enhancement of Underwater Propulsion Motor using Differential Evolution Optimization. *Indian Journal of Geo Marine Sciences*, 48(7), pp. 1113–1119.

Rupam, Marwaha, S. and Marwaha, A. (2022). FEA Based Design of Outer Rotor BLDC Motor for Battery Electric Vehicle. *International Journal of Electrical and Electronics Research*, 10(4), pp. 1130–1134.

Simcenter: MagNet Suite. https://www.plm.automation.siemens.com/global/en/products/simcenter/magnet.html.

Simón-Sempere, V., Simón-Gómez, A., Burgos-Payán, M. and Cerquides-Bueno, J.-R. (2021). Optimisation of Magnet Shape for Cogging Torque Reduction in Axial-Flux Permanent-Magnet Motors. *IEEE Transactions on Energy Conversion*, 36(4), pp. 2825–2838. doi: 10.1109/TEC.2021.3068174.

Wrobel, R. and Mellor, P. H. (2008). Design Considerations of a Direct Drive Brushless Machine with Concentrated Windings. *IEEE Transactions on Energy Conversion*, 23(1), pp. 1–8.

Yokoi, Y., Higuchi, T. and Miyamoto, Y. (2016). General Formulation of Winding Factor for Fractional Slot Concentrated Winding Design. *IET Electric Power Applications Journal*, 10(4), pp. 231–239.

Zhu, Z. Q. and Li, Y. X. (2018). Modularity Techniques in High Performance Permanent Magnet Machines and Applications. *CES Transactions on Electrical Machines and Systems*, 2(1), pp. 93–103.